



Volumetric effective cure shrinkage measurement of dual curable adhesives by fiber Bragg grating sensor

Sukrut Prashant Phansalkar¹ , Changsu Kim¹ , Bongtae Han^{1,*} , and Przemyslaw Jakub Gromala²

¹Mechanical Engineering Department, University of Maryland, College Park, MD 20742, USA

²Robert Bosch GmbH, Reliability Modeling and System Optimization (AE/ECU3), 72703 Reutlingen, Germany

Received: 25 March 2020

Accepted: 21 April 2020

Published online:

8 May 2020

© Springer Science+Business Media, LLC, part of Springer Nature 2020

ABSTRACT

A robust optical strain sensor, called fiber Bragg grating, is employed to measure the effective cure shrinkage—a part of cure shrinkage that is accumulated only after the gel point—of a dual cure adhesive during each stage of curing—(1) UV-curing stage and (2) thermal-curing stage. Unique experimental setups and procedures are developed and implemented to cope with the technical challenges associated with each stage of curing, including gel point detection and uniform curing. The effective cure shrinkage is measured to be 2.1% and 0.78% for acrylate compound (UV-curing) and two epoxy compounds (thermal-curing), respectively. The measurement accuracy of the proposed approach is corroborated by an additional measurement under the identical curing conditions. The results can be used to predict the cure-induced residual stresses of dual curable adhesives.

Introduction

Dual curable adhesives (DCAs) are widely used in applications where initial temporary alignment of components is needed before fixing parts permanently. The dual curing process yields two distinct and temporally stable sets of material properties during each stage of curing, which offers process flexibility.

An application utilizing a dual curing adhesive is illustrated in Fig. 1, where the DCA is applied to fix the lens barrel containing multiple singlets to the lens housing in a camera package. Alignment of the barrel with respect to the image sensor is required to ensure

proper focusing. The barrel is aligned in the lens housing, and it is fixed by UV-curing the adhesive within a few seconds or fraction of a minute. This stage is followed by subsequent thermal-curing for permanent fixing.

Several types of DCAs are available in the market for various applications. For example, acrylate–urethane-based adhesives have moisture resistance, and acrylate–epoxy-based adhesives have good adhesion strength and shock resistance [1]. The chemistry of the adhesives can be tailored to meet specific needs for applications [1–4].

The polymers undergo a significant reduction in volume during formation of covalent bonds (i.e.,

Address correspondence to E-mail: bthan@umd.edu

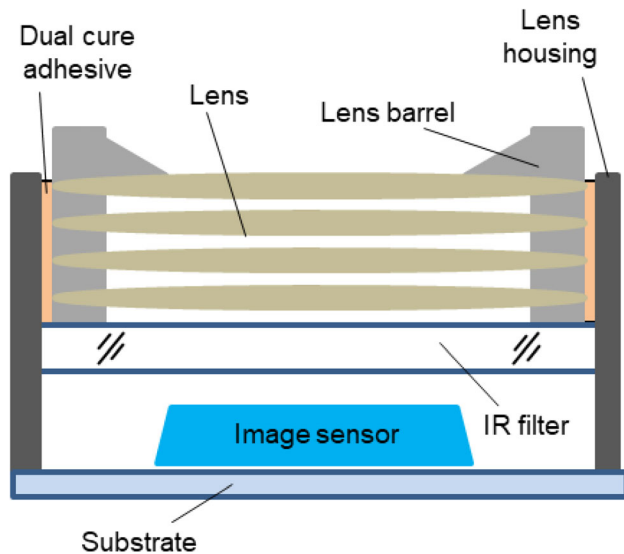


Figure 1 Schematic diagram of an integrated camera package where a dual cure adhesive is applied to fix the lens barrel containing lenses to the lens housing.

curing); this volumetric shrinkage is known as cure shrinkage [5]. It is important to note that the cure shrinkage occurs over the entire cure time, but the modulus of the polymer is virtually “zero” before the gel point. Thus, the cure shrinkage that occurs before this point does not contribute to the cure-induced residual stresses. The cure-induced residual stresses can be overestimated significantly if the total volumetric shrinkage is used in residual stress calculations. The cure shrinkage accumulated after the gel point is known as “effective cure shrinkage” [6, 7]. Only the effective cure shrinkage should be used to determine the cure-induced residual stresses.

The effective cure shrinkage of DCAs is required to predict the residual stress state of an assembly using DCA after curing is completed. This value has not been quantified because of the complex curing processes of DCAs, and this is the motivation of the study.

The objective of the paper is, thus, to measure the effective cure shrinkage of a DCA during each stage of curing—(1) UV-curing stage and (2) thermal-curing stage. An optical strain sensor called a fiber Bragg grating (FBG) has been used successfully to measure the effective cure shrinkage of a silicone-based elastomer [7]. In the method, an FBG was embedded in a cylindrically shaped specimen, and the strain caused by the effective cure shrinkage was continuously measured as a Bragg wavelength (BW) shift during

curing. The most critical challenge encountered during the measurement was to negate the effect of the mold that held uncured elastomer. The elastomer cured very slowly at room temperature, and this simple curing condition allowed to use an extremely flexible mold fabricated from plastic wrap to cope with the problem, whereby it deformed together with the elastomer during curing at room temperature. This simple solution is, however, not viable for DCA curing because of its much more complex curing conditions. Significant advancements are required to provide uniform UV-curing and high temperature curing. In addition, the effect of heat generation produced during the strong exothermic reaction of DCA curing has to be negated, which does not occur during elastomer curing.

The definition of the effective cure shrinkage and the fundamentals of the FBG-based method are reviewed briefly in “Background” section. The effective cure shrinkage measurements are reported in “Cure shrinkage measurements” section. The accuracy of measurements is discussed in “Discussion” section, and the paper is concluded with “Conclusions” section.

Background

The definition of the effective cure shrinkage is reviewed first. Then, the FBG-based method to measure the effective cure shrinkage is briefly described.

Effective cure shrinkage

During curing, relatively smaller molecules in polymers crosslink to form larger molecules. The micro-scale reduction in distance between molecules is seen as volume shrinkage at a macroscale, known as *cure shrinkage*. The cure shrinkage is proportional to the cure extent, which evolves nonlinearly with time.

The cure behavior of a typical polymer system is illustrated in Fig. 2, which shows the evolution of cure shrinkage, $\varepsilon(t)$, and elastic modulus, $E(t)$, normalized by their equilibrium values, as a function of time [6]. The figure also illustrates time at the gel point, t_{gel} , where the transition of an amorphous polymer from liquid to solid occurs due to gelation, and thus, the polymer starts developing mechanical strength (i.e., modulus).

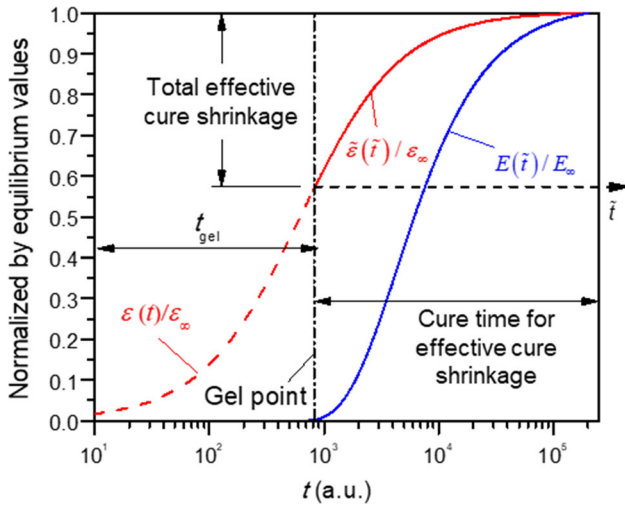


Figure 2 Illustration of evolutions of cure shrinkage and elastic modulus.

The time measured after the gel point is called as “effective time,” which is denoted as $\tilde{t} = t - t_{gel}$, and cure shrinkage that occurs after the gel point is called “effective cure shrinkage,” which is denoted as $\varepsilon(\tilde{t})$.

It should be noted that the gel point must be identified accurately for effective cure shrinkage measurements. This is the very reason why the FBG-based method described in the next section is ideal for measuring the effective cure shrinkage, because the FBG is a robust strain sensor that detects a volume change only associated with mechanical strains.

FBG-based method

A fiber Bragg grating (FBG) can be fabricated in a short segment of optical fiber (typically 5–10 mm). This is achieved by creating a periodic variation in the refractive index of the fiber core. When a broadband spectrum of light is incident on this region, only a narrow band of wavelength is reflected, which is centered on a fixed wavelength known as Bragg wavelength (BW or λ_B). The BW is related to the effective refractive index, n_{eff} , and pitch, A , of the grating [8] as:

$$\lambda_B = 2n_{eff}A \tag{1}$$

External loading and/or thermal excursion will alter the effective refractive index and the grating pitch, which causes a shift in BW. The total BW shift due to these loading conditions can be expressed as [5]:

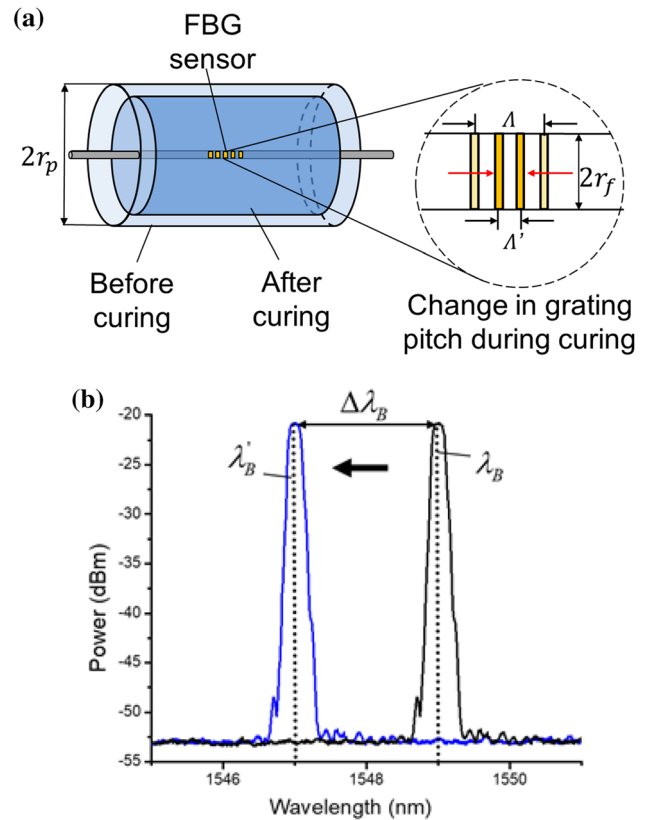


Figure 3 FBG-based method: **a** schematic diagram of a cylindrically shaped specimen before and after curing and **b** spectral power distributions showing the peak wavelength (i.e., Bragg wavelength) shift during curing.

$$\Delta\lambda_B = \Delta\lambda_i + \Delta\lambda_d \tag{2}$$

The first term, $\Delta\lambda_i$, is called the “intrinsic” BW shift, which is only caused by temperature change, which is defined as:

$$\Delta\lambda_i = \lambda_B \left(\alpha_f + \frac{1}{n_{eff}} \frac{dn}{dT} \right) \Delta T \tag{3}$$

where α_f , is the CTE of the fiber core material, n_{eff} is the effective refractive index, $\frac{dn}{dT}$, is the thermo-optic constant, and, ΔT , is the temperature change with respect to the initial condition. The second term, $\Delta\lambda_d$, is called the “deformation”-induced BW shift, which is caused by external stresses.

In the method, an FBG is first embedded at the center of a cylindrically shaped uncured polymer [5, 6]. As illustrated in Fig. 3a, volumetric shrinkage during curing will cause mechanical stresses in the fiber, which in turn alter the effective refractive index and pitch of the FBG. The inset illustrates the reduction of the pitch (A to A') caused by the

shrinkage. The net result is the BW shift from λ_B to λ'_B , as illustrated in Fig. 3b. The effective cure shrinkage can be determined from its relationship with the BW shifts [6].

It is important to recall that the shrinkage causing the stress in the FBG is “effective cure shrinkage” [6]. As discussed earlier, the polymer is in “liquid” state below the gel point, and this part of the shrinkage will not contribute to the stress.

The governing equation that provides the relationship was derived under the generalized plane strain condition with the following loading condition [6]:

$$\varepsilon_{\text{loading}} = \begin{cases} 0 & \text{for } 0 \leq r < r_f \\ \frac{\tilde{\varepsilon}}{3} & \text{for } r_f < r \leq r_p \end{cases} \quad (4)$$

where r_f and r_p are the radius of the fiber and the polymer, respectively; and $\tilde{\varepsilon}$ is the volumetric effective cure shrinkage.

The BW shift due to the above loading condition, i.e., the deformation-induced BW shift, $\Delta\lambda_d$, can be expressed as [6]:

$$\Delta\lambda_d = \frac{1}{E_f} \left\{ \begin{array}{l} \left[1 - \frac{n_{\text{eff}}^2}{2} (P_{12}(1 - \nu_f) - P_{11}\nu_f) \right] \sigma_{zz}^f - \\ \left[2\nu_f + \frac{n_{\text{eff}}^2}{2} ((1 - \nu_f)P_{11} - (1 - 3\nu_f)P_{12}) \right] \sigma_{rr}^f \end{array} \right\} \lambda_B \quad (5)$$

where λ_B is the initial BW; n_{eff} is the effective refractive index; σ_{zz}^f and σ_{rr}^f are the axial and radial stress components of fiber; ν_f is Poisson’s ratio of the fiber material; and P_{ij} are the strain optic constants.

The general form of the governing equation that provides the relationship can be expressed as:

$$\Delta\lambda_d = F(E_p, \beta) \cdot \frac{\tilde{\varepsilon}}{3} \quad (6)$$

where $\beta = \frac{r_p}{r_f}$ (called “configuration”) and $F()$ is the nonlinear function derived in Ref [6].

Cure shrinkage measurements

The effective cure shrinkage is measured separately for two stages: (1) UV-curing stage and (2) thermal-curing stage.

Specimen preparation

The dual cure adhesive (DCA) tested in this study consists of one acrylate and two epoxy resin compounds in the uncured mix. The acrylate component is trimethylolpropane acrylate (TMPTA), and epoxy components are bisphenol-A-epichlorohydrin (BPA) and bisphenol-F-epichlorohydrin (BPF) [1]. It also contains photoinitiators, latent curing agents, etc.

The curing mechanism of the DCA is illustrated in Fig. 4, which shows the adhesive chemistry after each curing stage. The acrylate monomers will cure first to form chains when exposed to UV light ($\lambda = 365$ nm). The epoxy oligomers will, then, cure in a subsequent thermal-curing process at elevated temperatures [1, 9].

Before the fiber was embedded in the uncured adhesive, the FBG was tested to obtain intrinsic properties. The bare FBG was placed in an oven, and the intrinsic BW was documented as a function of temperature. The intrinsic BW shift was fitted to a quadratic polynomial function with $\Delta T = T - 25^\circ\text{C}$ [6] as:

$$\Delta\lambda_i \text{ (nm)} = 0.01811 \cdot \Delta T + 9.96 \times 10^{-6} \cdot \Delta T^2 \quad (7)$$

The specimen size (or configuration) was decided based on the criteria of cure extent uniformity within the sample. Adhesive curing is an exothermic reaction, which produces heat. The heat generation in conjunction with low thermal conductivity can cause a large temperature gradient within the specimen, causing non-uniform curing.

A numerical analysis proposed in Ref. [6] was conducted to investigate the effect of heat generation on the cure extent uniformity. The total heat generation during curing was measured for the analysis

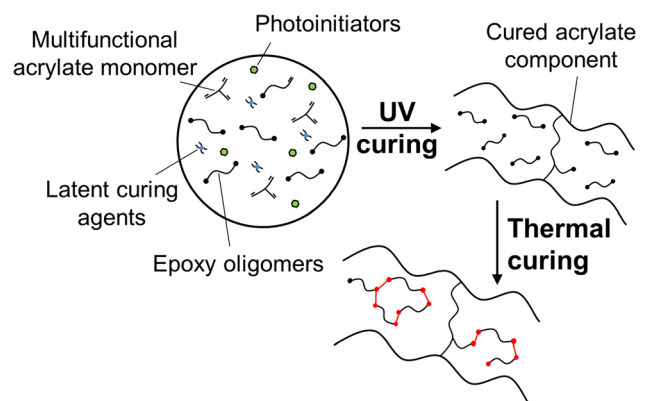


Figure 4 Illustration of curing mechanism of dual cure adhesive.

using a DSC temperature sweep experiment (5 °C/min). The results are shown in Fig. 5, where two heat generation peaks produced by two epoxy components are evident. The total heat generation was 156.7 J/g, and it was used as a heat generation input for the numerical analysis. The analysis indicated that the specimen configuration should be less than 30, i.e., $\beta = \frac{r_p}{r_f} < 30$, to ensure less than 1% non-uniformity between the center and edge of the specimen. This was used to set the upper limit of the configuration at a cure temperature.

The free-edge effect was also considered to determine the length of the specimen. A supplementary numerical analysis indicated that a length of 60 mm was enough to avoid the free-edge effect. More details about the free-edge effect can be found in Ref. [7].

UV-curing stage

The test setup used for UV-curing is illustrated schematically in Fig. 6, which shows the cylindrical housing containing a UV light source, the cylindrical mold containing the adhesive, acrylate plugs for fiber alignment, and V-groove fiber holders for holding the fiber in position.

Most metal, glass, and polymer tubes are opaque to UV light. Fluorinated ethylene propylene (FEP), a polymer of Teflon family, is commonly used in UV filtration systems, and it has a transmittance of > 90% over the wavelength of 300 nm [10]. A commercially available tube made of FEP was selected for the mold for UV-curing. The inner diameter (ID) and outer

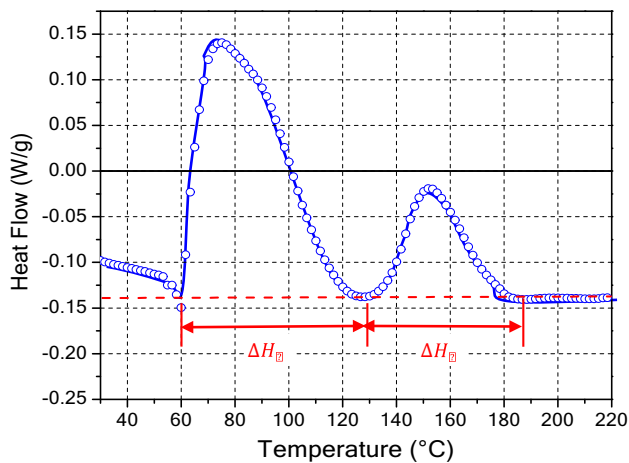


Figure 5 Results of DSC temperature sweep at 5 °C/min.

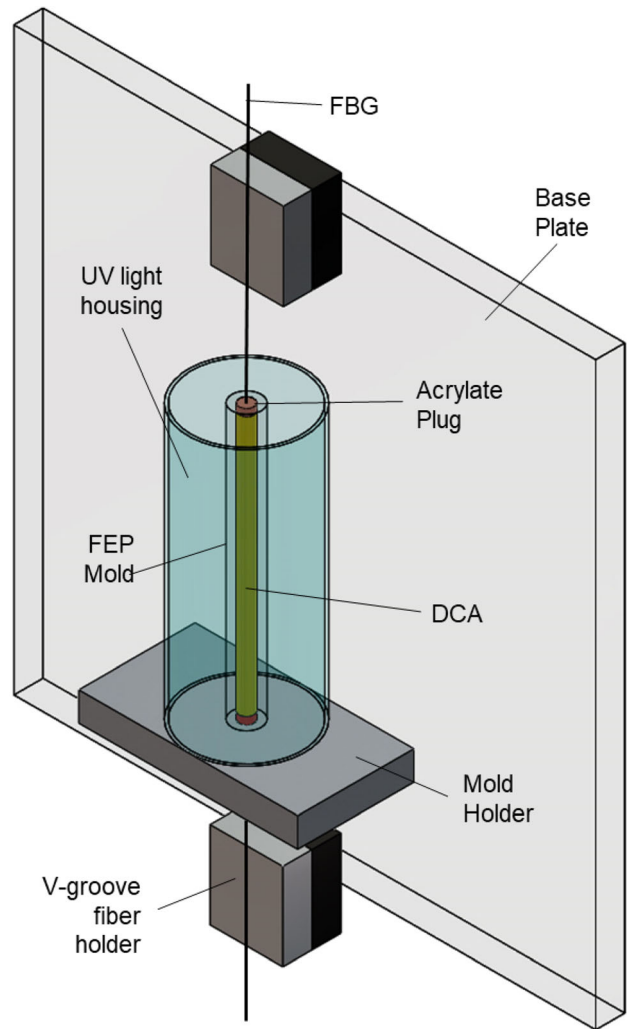


Figure 6 Schematic illustration of UV-curing setup.

diameter (OD) of the tube are 3.175 mm (0.125") and 6.35 mm (0.25"), respectively. Considering the fiber diameter of 125 μm, the tube provides a configuration of 25.4 ($\beta = 25.4$), which is smaller than the configuration upper limit described in the previous section.

A UV LED strip (Part 7021.65: Waveform Lighting) with the center wavelength of 365 nm was used as a UV light source. The penetration depth of the UV light at its maximum intensity (50 mW/cm²) was about 2 mm, which was sufficient for the specimen configuration. For uniform illumination during curing, the strip was wrapped around the inner surface of a custom-designed cylindrical housing. The LED strip and the housing are shown in Fig. 7. Very uniform light illumination along the entire mold was resulted.

Accurate alignment of the fiber in the mold was required to be use the governing equation (Eq. 5). This was achieved by two extra devices. In order to position the fiber at the center of the mold, an acrylate plug was fabricated using a laser cutting machine. The plug is shown in Fig. 8. The outer dimension of the plug was made identical to the ID of the mold. A tiny hole (155 μm in diameter) was made at the center to accommodate the fiber. The hole of the plug ensured accurate radial positioning of the fiber. The plug also served to retain the uncured adhesive inside the mold. The additional vertical alignment was achieved by the V-groove fiber alignment tool (HFV001: Thorlabs). The fiber was held in place in the groove using a tape (Fig. 6). The tape allowed for the fiber to remain in place without buckling while offering negligible resistance to the fiber movement in the axial direction.

Despite the relatively small configuration (3.175 mm), the temperature rise produced by the exothermic process during UV-curing was not ignorable. The temperature rise produced the intrinsic BW shift. This temperature effect had to be carefully compensated.

Since the UV test setup could not accommodate two molds, two separate tests were conducted to record the temperature rise and the BW shift during UV-

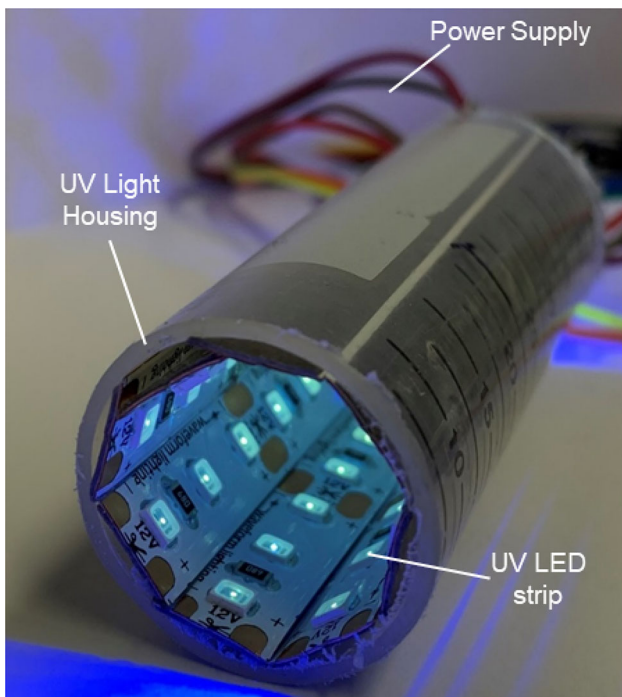


Figure 7 UV light housing where a UV LED strip is wrapped around the inner surface of a cylindrical tube.

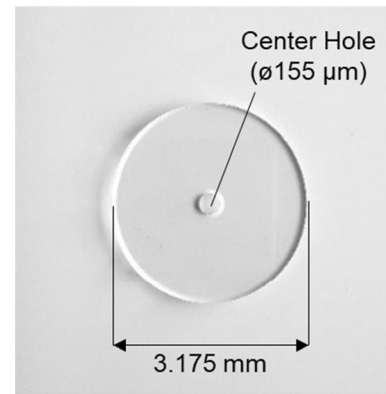


Figure 8 Acrylate plug used for the UV-curing mold.

curing, respectively. The first test was conducted using a DCA specimen with a thermocouple embedded at the center. The temperature history obtained from the first test is shown in Fig. 9. The temperature increased rapidly to 38.2 $^{\circ}\text{C}$ immediately after the LED was turned on, and it became stable and remained constant at 35.8 $^{\circ}\text{C}$ after approximately 50 s. The constant temperature was much higher than room temperature, which was caused by the radiative heat of the LED lamp. Only the temperature increase above the constant temperature ($\Delta T = 2.7$ $^{\circ}\text{C}$) was caused by heat generation during curing. It is important to note that thermal-curing at the stabilized temperature was virtually negligible. This will be explained in detail later using the DSC data.

The second test was conducted under the same condition using another DCA specimen with an FBG. The BW obtained from the second test is also shown in Fig. 9. The total BW shift obtained during UV-curing was determined from the BW data. The deformation-

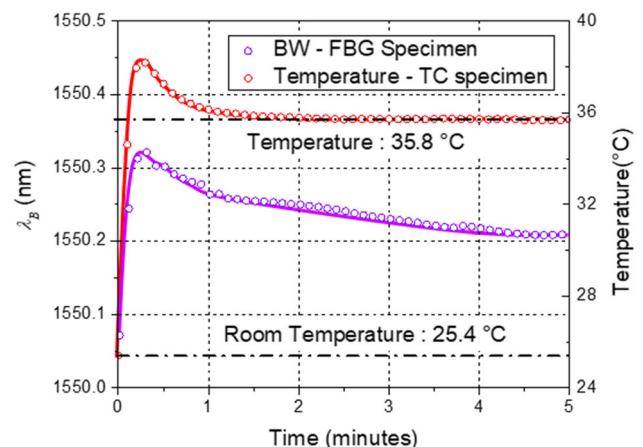


Figure 9 History of BW and temperature during UV-curing.

induced BW shift was, then, calculated by subtracting the intrinsic BW shift (Eq. 7) from the total BW shift. The three BW shifts are plotted in Fig. 10. It is important to note that the deformation-induced BW shift remained zero for the initial part of curing, from which the gel point was readily determined.

After the gel point, the deformation-induced BW shift continued to drop for approximately 4 min, beyond which the signal stabilized. UV exposure was continued for additional 30 s to ensure complete cure, and the light source was switched off. The stabilized signal confirmed completion of the UV-curing process. The deformation-induced BW shift accumulated during UV-curing is also shown in Fig. 10; it is 64 pm.

The mold tube has properties similar to Teflon, and it is not supposed to adhere to the acrylate that interacts with UV light. After UV-curing, the specimen was slipped out from the mold by itself, confirming this ideal non-sticky characteristic of the tube material. This also ensures that the effective cure shrinkage of the UV-curing process was measured under a constraint-free condition.

Thermal-curing stage

The DCA specimen removed from the UV-curing mold was cured further at 85 °C. The thermal-curing setup is illustrated schematically in Fig. 11, where both FBG and thermocouple embedded specimens prepared from the UV-curing stage are placed inside a convection oven (EC11A: Sun Electronic Systems).

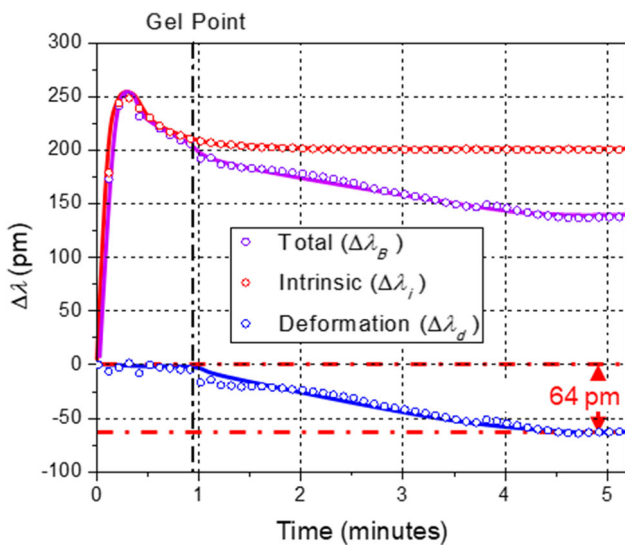


Figure 10 BW changes during UV-curing. The value shows the deformation-induced BW shift accumulated during UV-curing.

The convection oven was preheated until the thermocouple attached to the specimen seat reached 85 °C. Then, two specimens were inserted and placed on the specimen seat through a small hole built on the oven. This procedure offered negligible disturbance of the thermal equilibrium.

The temperature and the BW obtained from the two specimens are shown in Fig. 12. An overshoot by the exothermic process was observed (the maximum overshoot of 18 °C). The overshoot from the target temperature lasted for about 6.5 min, beyond which the temperature stabilized at 85 °C, and thus ensured isothermal curing.

The total, intrinsic, and deformation-induced BW shifts obtained during the initial part of thermal-curing are shown in Fig. 13. The gel point was determined as the end of the plateau region of the deformation-induced BW shift. The specimen cured continuously for approximately 43 h until no change in BW signal was observed. The deformation-induced BW shift over the entire thermal-curing stage is shown in Fig. 14, where a plateau region at the end is clearly seen indicating that curing process is completed. The deformation-induced BW shift

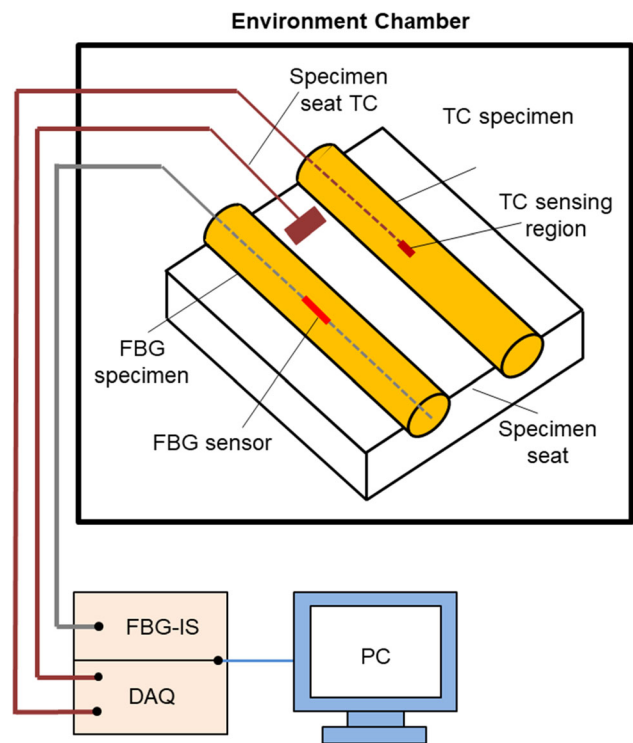


Figure 11 Schematic diagram of thermal-curing setup inside a convection oven.

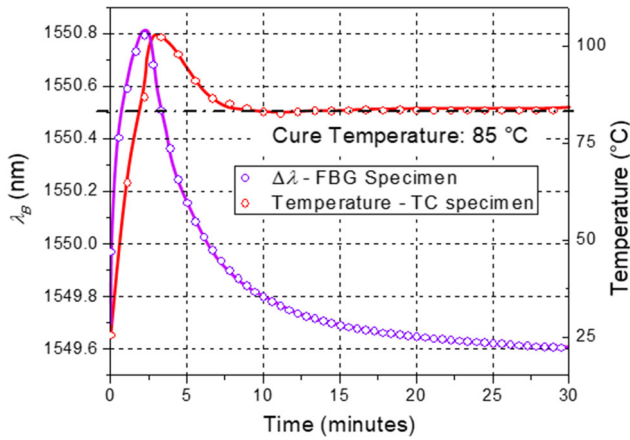


Figure 12 History of BW and temperature during thermal-curing.

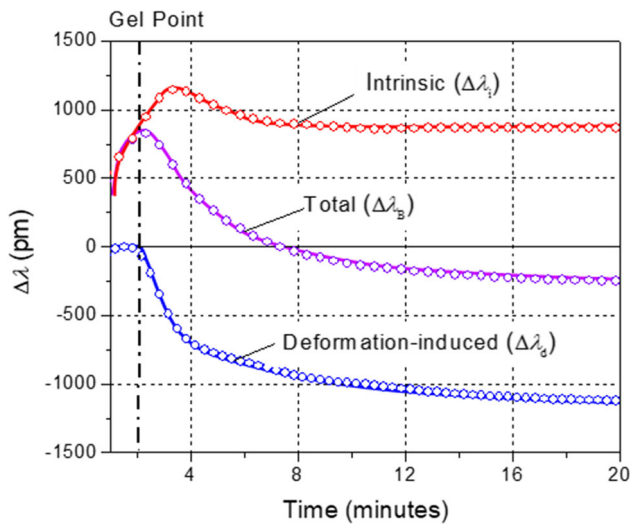


Figure 13 BW shifts during the initial part of thermal-curing.

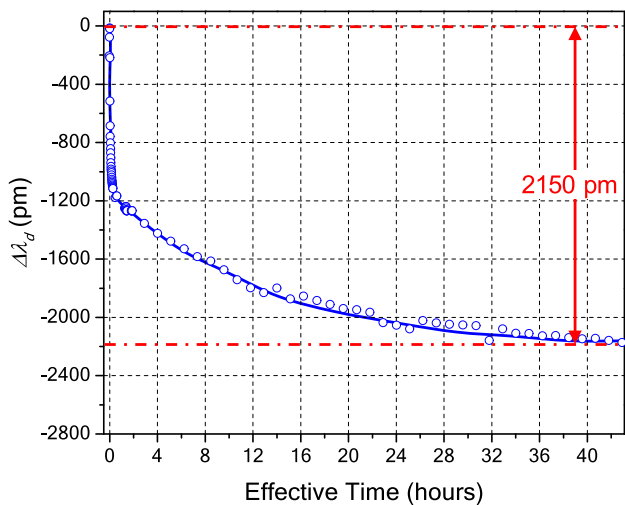


Figure 14 Deformation-induced BW shift during the entire period of thermal-curing.

accumulated during thermal-curing is also shown in Fig. 14; it is 2150 pm.

Calculation of effective cure shrinkage

It is important to recall that the equilibrium modulus is required to calculate the effective cure shrinkage from the deformation-induced BW shift (Eq. 6). The modulus of the UV-cured specimen was difficult to measure by the conventional test apparatus such as dynamic mechanical analyzer (DMA) due to its extremely low value. For this reason, the modulus values available in the literature were used for the calculation of UV-curing-induced effective cure shrinkage: 0.98 MPa [11], 1.04 MPa [12] and, 1.13 MPa [13]. Substituting the deformation-induced BW change of 64 pm (Fig. 10) and the representative modulus of 1.05 (± 0.08) MPa into Eq. (6), the volumetric effective cure shrinkage was determined to be 2.098 (± 0.017)%.

The modulus of the DCA specimen after thermal-curing was determined by a commercial DMA instrument. Three-point bending test results obtained at 85 °C are shown in Fig. 15. The modulus was obtained from the slope of the linear fit ($R^2 = 0.998$), and it was 247 MPa. Equation (6) was used again to calculate the effective cure shrinkage caused by thermal-curing using $\Delta\lambda_d = 2150$ pm and the equilibrium modulus. Considering the modulus uncertainty of 1% based on the specifications of the instrument (DMA RSA3), the volumetric effective cure shrinkage was determined to be $0.778 \pm 0.0024\%$.

Discussion

An additional experiment was conducted to investigate repeatability of the proposed testing procedure. The results obtained from the additional experiment are compared with the original test results in Fig. 16. Both UV-curing and thermal-curing-induced BW shifts are virtually identical, which confirms that the measurements can be done very consistently and accurately, albeit complex.

As mentioned earlier, the radiative heat produced by the LED lamp increased the base temperature of the specimen by approximately 10 °C (from 25.4 to 35.8 °C) during the UV-curing state. As can be seen from the DSC data (Fig. 5), the heat generation starts

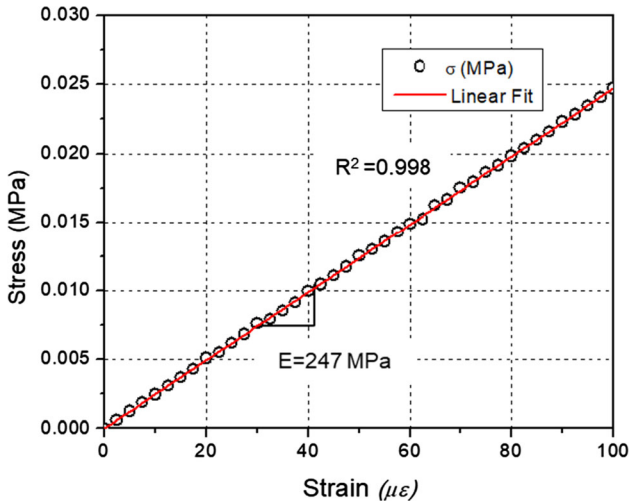


Figure 15 Stress versus strain relationship of DCA obtained at 85 °C.

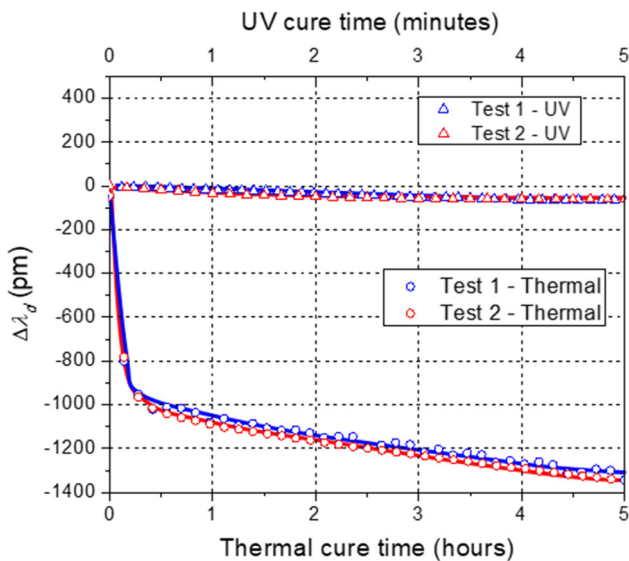


Figure 16 Deformation-induced BW change in Test 1 and Test 2 for UV-curing and thermal-curing.

around 60 °C, which is a clear indication that the epoxy components will not cure during the UV-curing stage.

It is worth noting that a clear change in slope was observed after approximately 30 min in the thermal-curing stage (Fig. 14). In the DSC data (Fig. 5), the heat generation of the first peak ($\Delta H_1 = 122.63 \text{ J/g}$) is much larger than that of the second peak ($\Delta H_2 = 34.06 \text{ J/g}$). It is speculated that the epoxy component associated with the first peak cures much faster at the thermal-curing temperature of 85 °C

compared to the epoxy component associated with the second peak, and thus produces the rapid change of the BW for the first 30 min of the thermal-curing stage. Each epoxy component could be tested separately to evaluate this effect more quantitatively.

Conclusions

A dual cure adhesive that consists of acrylate compound and two epoxy compounds was tested to measure the *effective cure shrinkage*—a part of cure shrinkage that solely contributes to cure-induced residual stresses. A robust optical strain sensor, called fiber Bragg grating (FBG), was employed to achieve the goal. Dual stage of curing—(1) UV-curing stage and (2) thermal-curing stage—posed unique technical challenges, but they were dealt with successfully by improvising unique experimental setups and procedures for each stage of curing. The amounts of the effective cure shrinkage were determined to be 2.1% and 0.78% for the acrylate compound (UV-curing) and two epoxy compounds (thermal-curing), respectively. Measurement accuracy and repeatability were confirmed by an additional test. The proposed test procedure can be used other types of dual cure adhesives. Conventional methods which measure total volumetric shrinkage can significantly overestimate the residual stresses. To the best of author’s knowledge, no previous methods have measured effective cure shrinkage for DCA needed to evaluate residual stresses.

Acknowledgements

This work was supported by the Center for Advanced Life Cycle Engineering (CALCE) of the University of Maryland. Their support is gratefully acknowledged.

Compliance with ethical standards

Conflict of interest No conflict of interest exists in regard to preparation of this manuscript.

References

[1] Park Y-J, Lim D-H, Kim H-J, Park D-S, Sung I-K (2009) UV-and thermal-curing behaviors of dual-curable adhesives

- based on epoxy acrylate oligomers. *Int J Adhes Adhes* 29:710–717
- [2] Tumbleston JR, Shirvanyants D, Ermoshkin N, Januszewicz R, Johnson AR, Kelly D, Chen K, Pinschmidt R, Rolland JP, Ermoshkin A (2015) Continuous liquid interface production of 3D objects. *Science* 347:1349–1352
- [3] Konuray O, Fernández-Francos X, Ramis X, Serra À (2018) State of the art in dual-curing acrylate systems. *Polymers* 10:178–202
- [4] Austermann J, Redmann AJ, Dahmen V, Quintanilla AL, Mecham SJ, Osswald TA (2019) Fiber-reinforced composite sandwich structures by Co-curing with additive manufactured epoxy lattices. *J Compos Sci* 3:53–66
- [5] Wang Y, Han B, Kim D, Bar-Cohen A, Joseph P (2008) Integrated measurement technique for curing process-dependent mechanical properties of polymeric materials using fiber Bragg grating. *Exp Mech* 48:107–117
- [6] Wang Y, Woodworth L, Han B (2011) Simultaneous measurement of effective chemical shrinkage and modulus evolutions during polymerization. *Exp Mech* 51:1155–1169
- [7] Sun Y, Han B, Parsa E, Dasgupta A (2014) Measurement of effective chemical shrinkage and equilibrium modulus of silicone elastomer used in potted electronic system. *J Mater Sci* 49:8301–8310. <https://doi.org/10.1007/s10853-014-8538-z>
- [8] Hill KO, Meltz G (1997) Fiber Bragg grating technology fundamentals and overview. *J Lightwave Technol* 15:1263–1276
- [9] Park J-W, Shim G-S, Lee J-G, Jang S-W, Kim H-J, Choi J-N (2018) Evaluation of UV curing properties of mixture systems with differently sized monomers. *Materials* 11:509–523
- [10] Chen S, Huang C, Jiang X, Luo X, Fang Y, Wu W (2016) The transmittance, transmittance wavefront, and laser induced damage properties of thin fluoride polymer films may be used as short pulse laser debris shields. *Int J Polym Sci* 2016:1367537
- [11] Babu RR, Singha NK, Naskar K (2009) Dynamically vulcanized blends of polypropylene and ethylene-octene copolymer: comparison of different peroxides on mechanical, thermal, and morphological characteristics. *J Appl Polym Sci* 113:1836–1852
- [12] Hopper AV (2007) Recent developments in polymer research. Nova Publishers, New York
- [13] Holt T (2011) Cure-on demand wood adhesives using frontal polymerization of acrylates. Master's thesis, Louisiana State University

Publisher's Note Springer Nature remains neutral with regard to jurisdictional claims in published maps and institutional affiliations.